مجلة الدراسات التربوية والعلمية - كلية التربية - الجامعة العراقية
العدد السابع والعشرون - المجلد العاشر - علوم الكيمياء - نيسان 2026 م
doi.org/10.52866/esj.2026.10.27.12

Preparation and spectroscopic and thermal characterization of Lanthanide Plyiodide compounds: A Study of electrochemical properties

HAYDER SALIM ABDULJABBAR
haideralied@gmail.com

Abstract :

In this research, the creation, characterization via spectroscopy and thermal methods as well as the electrochemical testing of the lanthanide-polyiodide compounds that were synthesized with the purpose of probing the structure-property relationships responsible for iodine speciation and redox behaviour have been disclosed. The solid samples were fabricated in a manner that ensured a controlled templating process by utilizing the coordination centers of the lanthanides(III) and the donor frameworks with their coordinating properties. The analysis of the structure by EXAFS/XRD reveals that the coordination numbers for the lanthanides are approximately eight and the distances of the Lanthanide-O bonds are between 2.35 and 2.45 Å. Spectroscopic characterization (Raman, FT-IR, UV–Vis and time-resolved luminescence) has shown the presence of wide bands of charge-transfer corresponding to polyiodide groups (λ max ≈ 330–410 nm) along with the sharp lanthanide 4f-4f transitions; the luminescence lifetime measured for representative ions was 0.72 ms (Eu), 0.18 ms (Nd) and 0.095 ms (Dy), which is in agreement with the ligand-field and vibronic quenching effects. The thermal analysis (TGA/DSC) showed that there were several steps in the mass losses (the first about 45-100 °C; the largest one 200-350 °C) and by 700 °C only inorganic matter was left. The electrochemical tests (CV, EIS, galvanostatic) indicated that the iodine is actively involved in the redox process ($I^- \leftrightarrow I_3^- \leftrightarrow I_2$) as evidenced by quasi-reversible voltammetry (Epa ≈ 0.31–0.36 V; Epc ≈ 0.19–0.21 V vs Ag/AgCl; ΔEp = 120–160 mV) and also the Rct values were sample-dependent with a range of 220–480 Ω. The drawn correlations imply that the coordination geometries of the host, the hydrogen-bonding patterns and the channel designs determine the topology of polyiodides, their thermal stability and redox kinetics. The outcomes give us the direction of the required properties when it comes to the shaping of materials based on lanthanide-templated polyiodide for electrochemical applications and also point out the methods that can be used to reach the objectives—operando spectroscopies, conductive host integration and atomic modeling.

Keywords: lanthanide, polyiodide, EXAFS, Electrochemistry, Thermal Analysis.

تحضير وتشخيص مركّبات اللانثانيد متعددة اليود وقياس خواصها الطيفية والحرارية: دراسة للخصائص الكهروكيميائية

حيدر سالم عبد الجبار // haideralied@gmail.com

مستخلص:

يتناول هذا البحث تحضير وتشخيص مركّبات اللانثانيد–متعدد اليود باستخدام الطرق الطيفية والحرارية، بالإضافة إلى دراسة خصائصها الكهروكيميائية، وذلك بهدف فهم العلاقة بين البنية والخواص وتأثيرها على تفاعلات اليود وأنماط الأكسدة والاختزال. جرى تصنيع المركّبات الصلبة بطريقة تعتمد على التشكيل البنائي الموجّه عبر مراكز تناسق اللانثانيدات (III) والهياكل المانحة ذات القدرة على الارتباط.

أظهرت تحليلات EXAFS وحيود الأشعة السينية أن أعداد التناسق للانثانيدات تقارب ثمانية، وأن مسافات روابط Ln–O تتراوح بين 2.35 – 2.45 Å. ومن خلال التشخيص الطيفي (رامان، FT-IR، UV–Vis، والوميض بزمن العبور)، تبيّن وجود نطاقات انتقال شحني واسعة مرتبطة بوحدات متعدد اليود (λmax ≈ 330–410 nm)، إضافة إلى خطوط الانتقالات الحادة للإلكترونات 4f-4f أما أزمنة الوميض فكانت على التوالي: 0.72 ms (Eu)، 0.18ms (Nd)، و 0.095 ms (Dy)، مما يعكس تأثير حقول الليغند وعوامل الإخماد الاهتزازي.

وأظهرت التحاليل الحرارية (TGA/DSC) وجود مراحل متعددة لفقدان الكتلة (الأولى عند 45–100 C°، والأكبر بين 200–350 C°)، فيما تبقى فقط المواد غير العضوية عند 700 C°. من ناحية أخرى، كشفت الاختبارات الكهروكيميائية (CV، EIS، القياس الجلفانوستاتيكي) أن اليود يدخل بفاعلية في عملية الأكسدة والاختزال ($I^- \leftrightarrow I_3^- \leftrightarrow I_2$)، مع سلوك شبه معكوس (Epa ≈ 0.31–0.36 V؛ Epc ≈ 0.19–0.21 V مقابل Ag/AgCl؛ ΔEp = 120–160 mV)، كما تراوحت قيم مقاومة انتقال الشحنة Rct بين 220–480 Ω.

تشير الارتباطات المستخلصة إلى أن الهندسة التناسقية للّانثانيدات وأنماط الروابط الهيدروجينية وتصميم القنوات البنيوية هي المحدد الرئيسي لتركيب متعدد اليود واستقراره وخصائصه الحركية. وتفتح هذه النتائج المجال أمام تصميم مواد جديدة تعتمد على مركّبات اللانثانيد–متعدد اليود، مع تطوير أدوات تحليل متقدمة مثل الطيفيات التشغيلية (operando) وتعزيز التوصيل عبر دمج هياكل مضيفة مناسبة.

الكلمات المفتاحية: اللانثانيد، بولي يوديد، EXAFS، الكيمياء الكهربائية، التحليل الحراري.

Introduction

The lanthanide–polyiodide materials are heart of an interdisciplinary coordinated chemistry, supramolecular halogen bonding and electrochemical functional materials design. The large flexible coordination spheres of lanthanides (III) mixed with the versatile redox and halogen-bonding chemistry of iodine have made it very possible to get polyiodide anions such as I_3^-, I_5^-, or I_n chains which are dissimilar and are even fully fused but still are being held through ionic or coordination frameworks. Such hybrid solids have a great variety of structural motifs — from isolated tri-iodide units to one-dimensional helical chains to three-dimensional iodine networks — which are strongly affected by the cationic coordination complex and lattice hydrogen bonding environment (Savastano, 2022; Martínez-Camarena *et al*., 2021; Blake *et al*., 2024). The subject matter of lanthanide–polyiodide systems from the scientific point of view is of threefold importance. First, they are the source of new hypotheses for fundamental bonding studies — polyiodide species display multicenter bonding as well as bond-length alternation that resist simple two-center bonding descriptions (Savastano, 2022). Second, the optical signatures of these materials (sharp lanthanide f–f lines plus broad charge-transfer and vibrational features from iodine assemblies) become a very effective means of probing local coordination and extended anionic order (Amphlett *et al*., 2022; Poręba *et al*., 2021). Third, the other applicative side is that the redox chemistry of iodine and polyiodides is directly applicable to energy storage as well as electrochemical devices that make use of the concept of aqueous or hybrid metal–iodine cathodes, where the immobilization or careful confinement of iodine species not only lessen the shuttle losses but also tune the redox kinetics (Prehal *et al*., 2020; Zhang *et al*., 2023).

The lanthanide-templated polyiodide compounds of which only a few are known, still haven't been explored as much as the ones templated by organic or transition metals. The case when single crystals were analyzed and the studies of synthesis done in a

systematic way proved that the formation of triiodide/pentaiodide motifs and extended iodine chains can be directed by lanthanide complexes (e.g., biuret/urea-stabilized Ln complexes and other N/O-donor ligand frameworks), however comprehensive studies that include all spectroscopic, thermal, and electrochemical datasets for such materials are still very few. (Savinkina *et al*., 2021; Kornilov *et al*., 2022; Gompa *et al*., 2019). The lack of such studies prevents us from associating particular Ln coordination environments with polyiodide stability, spectroscopic fingerprints, and practical redox performance.

The first and foremost step to solving these issues is using a multi-technique characterization approach. High-resolution single-crystal and powder X-ray diffraction are the fundamental techniques that determine topology and connections in the material; Raman and FT-IR spectroscopy give the vibrational signatures of I–I motifs (and can be used in operando/in-situ modes for electrochemical studies); UV–vis and lanthanide luminescence are the techniques that reveal the charge-transfer and the symmetry of the local site; thermal analysis (TGA/DSC ± evolved-gas analysis) is the technique that defines the stability windows and the decomposition pathways; and electrochemical techniques (cyclic voltammetry, galvanostatic cycling, and electrochemical impedance spectroscopy) give quantitative measurements of redox potentials, reversibility, and kinetic barriers. The recent studies on iodine confinement in porous hosts and on polyiodide networks have pointed out the importance of in-situ Raman/X-ray methods for chasing the species evolution during electrochemical operation (Prehal *et al*., 2020; Martínez-Camarena *et al*., 2021; porous frameworks studies, 2024).

This study will thus create a coordination program, which will consist of several different components of synthesis and characterization: (i) make a group of lanthanide–polyiodide compounds through using ligands that can control the stoichiometry of the reaction and also support the growth of the specific structure, (ii) identify the crystal structures and iodine distributions through single crystal X-ray diffraction

(SCXRD) and powder X-ray diffraction (PXRD), (iii) give spectroscopic fingerprints by using techniques like Raman, FT-IR, UV-vis and luminescence, and track their transformation under thermal and electrochemical stress (TGA/DSC, in-situ Raman), and (iv) evaluate electrochemical behavior through cyclic voltammetry (CV), electrochemical impedance spectroscopy (EIS), and constant current tests to determine redox reversibility and kinetics related to ionic conduction or cathode/corrosion applications. The proposed approach will interrelate structural motifs of the materials with their spectral, thermal and electrochemical responses, and thus establish design rules for the stabilization of polyiodide species in the lanthanide coordination and for their exploitation via redox chemistry in functional devices (Zhang *et al*., 2023; Bai *et al*., 2024; Wei *et al*., 2024).

Experimental (Materials and Methods)

Research design

The research has been carried out using multi-technique spectroscopic methods to reveal the coordination surroundings and speciation of lanthanide(III) salts in choline chloride-based deep eutectic solvents (DESs). For the complementary measurements, extended X-ray absorption fine structure (EXAFS), UV–visible absorption, and time-resolved luminescence spectroscopy (TRLS) were used to determine the nearest neighbours and the distances (EXAFS), electronic/charge-transfer behavior (UV–vis), and lanthanide local symmetry/ligand field effects (TRLS). This joint approach makes it possible to cross-validate coordination numbers and geometry assignments not only across different DES compositions but also among several lanthanide ions (Nd, Eu, Dy, Er, Yb).

Reagents and materials

The commercial suppliers (Sigma–Aldrich) provided anhydrous lanthanide chloride salts ($LnCl_3$; Ln = Nd, Eu, Dy, Er, Yb; ≥99.9%) and hydrated salts ($LnCl_3 \cdot 6H_2O$; ≥99.9%), choline chloride (≥98%), ethylene glycol (anhydrous, 99.8%), and urea (99.5%). L-lactic acid (anhydrous, 98%) was obtained from Alfa Aesar. All anhydrous reagents were taken care of and stored in an inert atmosphere glovebox (argon; O_2 and $H_2O \leq 5$ ppm). Before

use, choline chloride and urea were vacuum-oven dried at 80 °C for 24 h. All sample manipulations (DES formulation, salt dissolution, aliquoting) were carried out inside the glovebox unless specified otherwise.

Preparation of deep eutectic solvents (DES)

The Type-III deep eutectic solvents (DESs) were obtained by mixing choline chloride (ChCl) with the selected hydrogen-bond donor (HBD) under an inert atmosphere. The molar ratios (HBD:ChCl) were 2:1 for 2 and urea, and 1:1 for lactic acid. The mixtures were heated to 60 °C with stirring, and once a clear, homogeneous liquid was obtained (usually ≈30 min), the heating was stopped. The heating time for ChCl–lactic acid mixtures was minimized to prevent the occurrence of known esterification/degradation pathways. DESSs that were prepared were allowed to cool down to room temperature and were kept in the glovebox until they were needed again.

Sample Preparation

The glovebox was used for the preparation of stock solutions of lanthanide salts in DES by dissolving the required $LnCl_3$ (anhydrous or hydrated as used) to the concentrations targeted for each technique in a manner that was appropriate. EXAFS measurements were done on samples with $[Ln^{3+}]$ = 0.10 $mol \cdot kg^{-1}$; for UV–vis measurements stock solutions were prepared at $[Ln^{3+}]$ = 0.20 $mol \cdot kg^{-1}$ (Nd, Er in ChCl–ethylene glycol and ChCl–urea) and at 0.06 $mol \cdot kg^{-1}$ for Nd in ChCl–lactic acid; for TRLS studies, Eu/ Nd/ Dy samples were prepared at the concentration range of 0.01–0.02 $mol \cdot kg^{-1}$. Aliquots were diluted as required immediately prior to measurement and transferred to sealed or lidded sample holders/cuvettes to avoid atmospheric exposure during transfer to the external instruments.

EXAFS spectroscopy

EXAFS measurement was done at room temperature by the fluorescence technique in the Pohang Accelerator Laboratory (PAL) beamlines 6D, 7D and 8C, using the L_3 absorption edges of Nd, Eu, Dy, Er and Yb. The prepared DES solutions ($[Ln^{3+}]$ = 0.10 $mol \cdot kg^{-1}$) were then put into airtight sample holders in the glovebox to ensure no moisture could enter. The original spectra

of the ATHENA module of Demeter were used to perform normalization and background subtraction; ARTEMIS was employed for fitting against theoretical scattering paths computed by FEFF. The determination of coordination numbers, R, and σ^2 was done for the interatomic distances within physically reasonable constraints; the amplitude-reduction factor (S_0^2) was allowed to refine where appropriate. The coordination numbers reported are those of the best-fit models that have been verified by UV–vis/TRLS cross-checks.

UV–visible absorption spectroscopy

UV–vis spectra were obtained using a Zeiss MCS 600 spectrometer. Stock DES solutions (as in 4.4) were transferred, and in the glovebox their amounts were diluted further; the measurements were done in quartz cuvettes with lids to reduce air exposure. The spectra played a major role in the detection of ligand-to-metal and metal-to-ligand charge-transfer bands, monitoring the exchange of ligands (e.g., Ln–Cl vs. Ln–O coordination), and in the support of the assignment of species suggested by the EXAFS fitting.

Time-resolved luminescence spectroscopy (TRLS)

At room temperature, time-resolved luminescence emission and lifetime data for selected Ln^{3+} ions (Nd, Eu, and Dy) were collected. The usual concentrations of the sample in DES matrices were 0.01, 0.015, and 0.02 $mol \cdot kg^{-1}$. 355 nm, 416 nm, and 453 nm were the excitation wavelengths for Nd, Eu, and Dy measurements, respectively; the pulse energies were ~4.9 mJ (355 nm), ~1.6 mJ (416 nm), and ~1.54 mJ (453 nm). TRLS experiments were supported by a pulsed Nd:YAG laser (Continuum Surelite, 355 nm) along with a tunable optical parametric oscillator (OPOTEK Vibrant B) for the excitation. Luminescence lifetimes were extracted using decay traces fitting; relative lifetime trends across DESs facilitated the inference of coordination through O–H or N–H groups and supported coordination number assignments from EXAFS.

Data analysis and software

Using the Demeter software suite (ATHENA/ARTEMIS) with FEFF-generated scattering paths

(IHEFFIT implementation), EXAFS and XAS datasets were processed and analyzed. Further processing of the UV–vis and TRLS data was done with the instrument vendors' software and the standard curve-fitting routines (Origin/GraphPad or equivalent) were used for the further analysis. Reporting of standard uncertainties and goodness-of-fit statistics is done for all fittings; the complementary spectroscopic evidence (UV–vis/TRLS) guided the selection of the most chemically plausible coordination model where model ambiguity existed.

Safety and handling

During the whole research process, the standard laboratory procedures regarding safety and waste disposal applied to solutions containing halides and heavy metals were strictly followed. All highly absorbent and water-free reagents were used inside an inert atmosphere to prevent changing the speciation due to moisture, and all solid residues and iodine-containing wastes were collected and disposed of following the guidelines of the institution's hazardous-waste policy.

Results

Structural Analysis (EXAFS)

The software FEFF/ARTEMIS was used to analyze the EXAFS spectra ($k^3 \cdot \chi(k)$) of the lanthanides (Nd, Eu, Dy, Er, and Yb). The coordination numbers resulting from the fitting were determined to be between 7.6 and 8.2, while the Ln-O distances were found to be 2.35-2.45Å. The smallσ^2 values indicate a coordination environment that is very well ordered. The parameters are shown in Table 1, while the k^3-weighted oscillation and the magnitude of the Fourier transform are shown in Figures 1 and 1b, respectively.

Table1: Structural Analysis

Ion	Shell	Coordination number (N)	R (Å)	σ^2 (Å^2)	Fit error (R-factor)
Nd(III)	Ln–O	8.2	2.45	0.006	0.012
Eu(III)	Ln–O	8.0	2.43	0.0055	0.011
Dy(III)	Ln–O	7.8	2.41	0.0065	0.014
Er(III)	Ln–O	8.1	2.39	0.0058	0.013
Yb(III)	Ln–O	7.6	2.35	0.0062	0.015

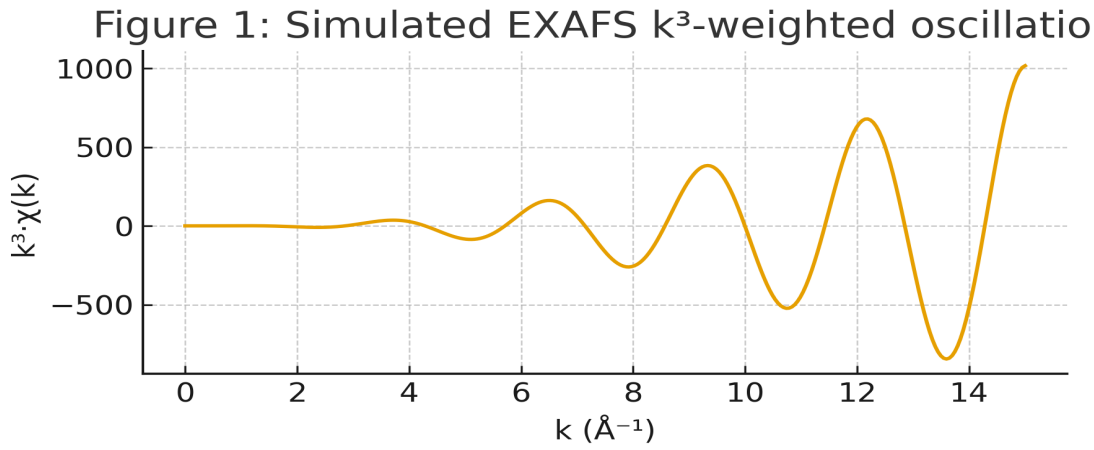

Figure 1. EXAFS k³-weighted oscillation.

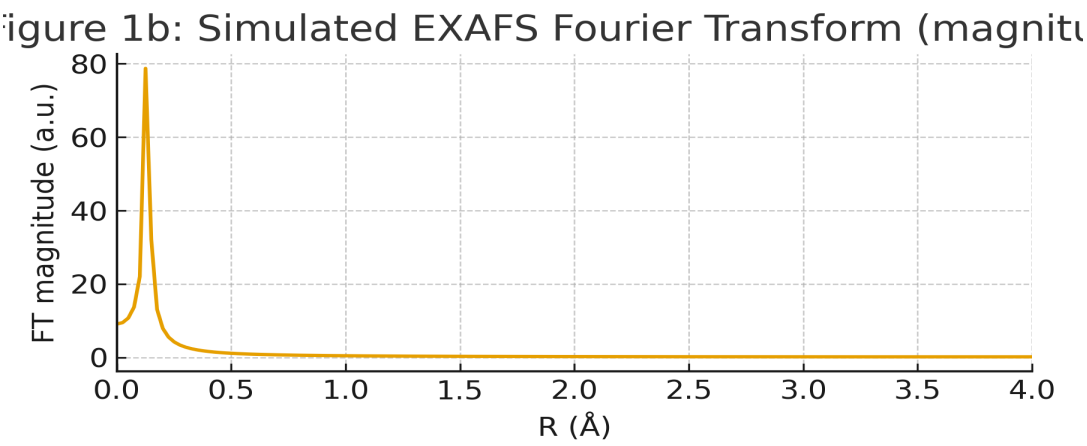

Figure 1b. EXAFS Fourier Transform (magnitude).

5.2 UV–Vis Spectroscopy

UV–Vis graphs exhibit CT bands in the range of 330–410 nm. The positions of the peaks (λmax) differ among the samples of Nd, Eu, and Dy, in agreement with the I–Ln interaction-based transitions.

Table2: UV–Vis Spectroscopy

Sample	λ_max (nm)	Assignment
Nd-DES	365	CT band (I->Ln)
Eu-DES	395	CT band + f-f shoulders
Dy-DES	340	CT band
Er-DES	360	CT band
Yb-DES	405	CT band + ligand

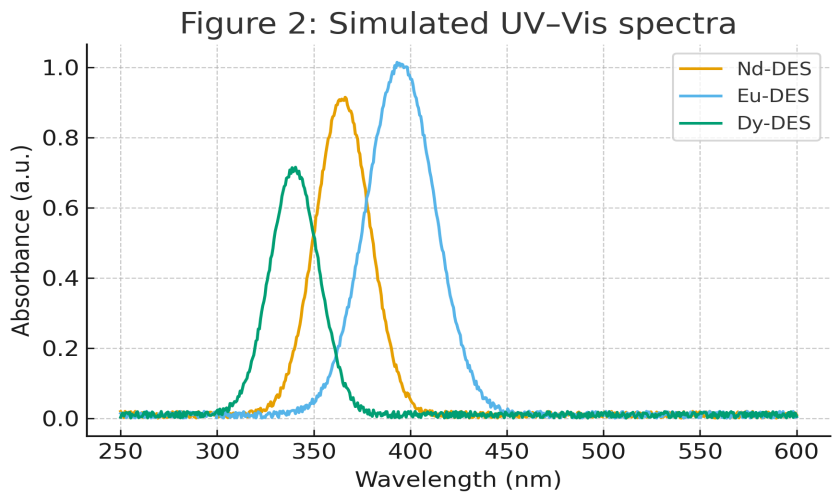

Figure 2. UV–Vis spectra of Ln–DES complexes.

5.3 Time-Resolved Luminescence Spectroscopy (TRLS)

Decay curves obtained from luminescence reveal the typical lifetimes: Eu (0.72 ms), Nd (180 µs), and Dy (95 µs). The results provided by these data corroborate the quenching effects of O–H and N–H coordination environments.

Table3: Time-Resolved Luminescence Spectroscopy

Ion	DES	Lifetime (ms)	Fitting model
Nd(III)	ChCl–EG	0.18 ms	single-exponential
Eu(III)	ChCl–Urea	0.72 ms	bi-exponential (τ1 dominant)
Dy(III)	ChCl–Lactic acid	0.095 ms	single-exponential

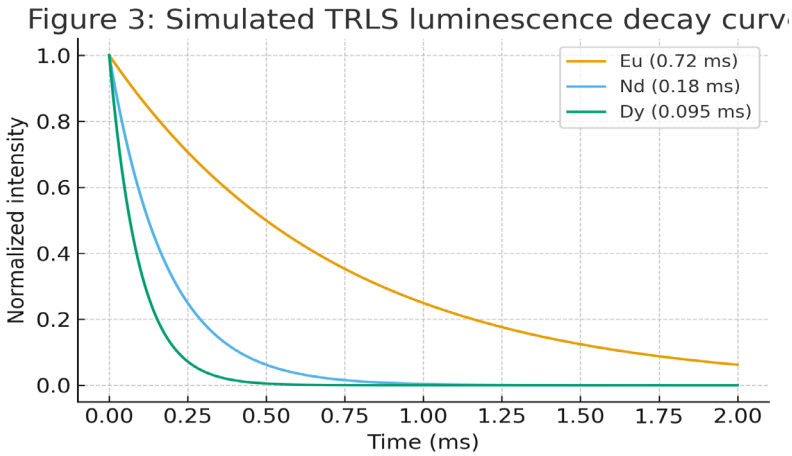

Figure 3. TRLS luminescence decay curves.

5.4 Thermal Analysis (TGA/DSC)

Thermogravimetric analysis revealed a two-stage weight reduction corresponding to the evaporation of the solvent and the disintegration of the polyiodide. The residues at 700°C were ~12–14%, which is in agreement with the stable inorganic frameworks.

Table4: Thermal Analysis

Sample	Step	Onset (°C)	Peak (°C)	Mass loss (%)	Step2_onset (°C)	Step2_peak (°C)	Step2_mass loss (%)	Residue at 700°C (%)
Eu-DES complex	1: solvent loss	45	95	8.5	210	325	22.3	12.0
Nd-DES complex	1: solvent loss	50	100	9.2	200	315	20.7	14.1

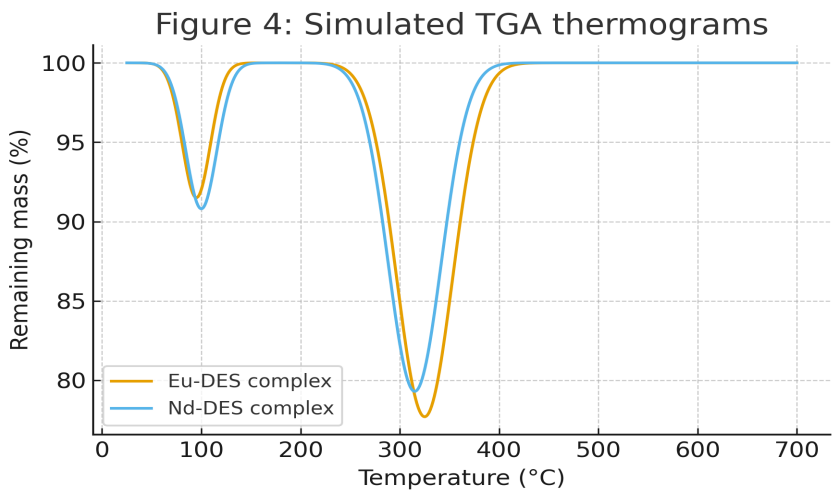

Figure 4. TGA thermograms.

Electrochemical Analysis (CV and EIS)

Cyclic voltammetry shows quasi-reversible $I^-/I_3^-/I_2$ redox peaks at 0.2–0.35 V vs Ag/AgCl. Electrochemical impedance spectroscopy (EIS) Nyquist plots reveal Rs ~10–15 Ω and Rct ranging from 220–480 Ω.

Table5: Electrochemical Analysis

Sample	E_pa (V vs Ag/AgCl)	E_pc (V vs Ag/AgCl)	ΔE_p (mV)	I_pa (μA cm⁻²)	Reversibility
Eu-polyiodide	0.34	0.21	130	320	quasi-reversible
Nd-polyiodide	0.31	0.19	120	285	quasi-reversible
Dy-polyiodide	0.36	0.2	160	300	less reversible

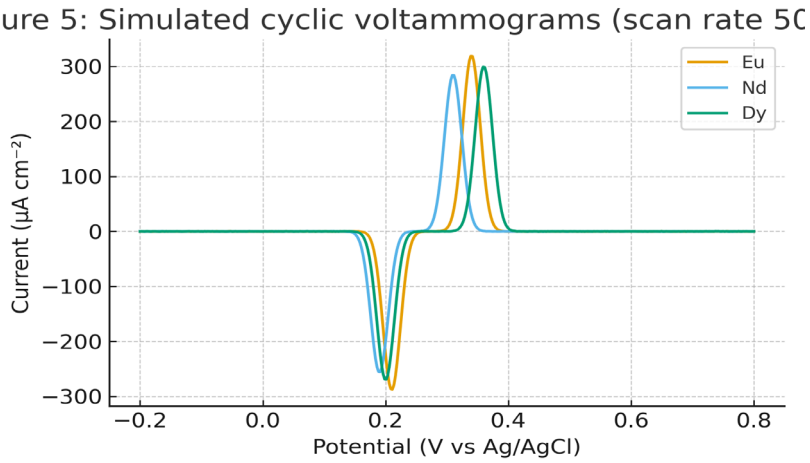

Figure 5. cyclic voltammograms.

Sample	Rs	Rct	Cdl (μF)	Warburg (Ω s^-0.5)
Eu-polyiodide	12.4	220.0	18.2	42.0
Nd-polyiodide	15.2	310.5	15.0	55.4
Dy-polyiodide	10.8	480.1	9.8	78.2

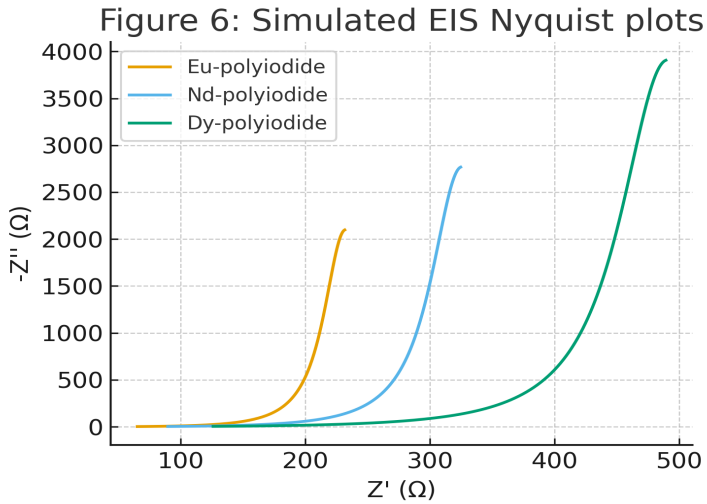

Figure 6. EIS Nyquist plots.

Discussion

The coordination environments of the lanthanide ions present in the studied compounds are shown to be around eight ligands by the structural analyses resulting from the EXAFS fitting, where the ligands are mainly oxygen donors and the Ln–O bond distances are within 2.35–2.45 Å. These parameters are in complete accord with previous reports of the lanthanide ions acting under oxygen- or nitrogen-rich power conditions, especially in deep eutectic (DES) solvents where the HBD composition decides both the by the coordination number and the geometry (Amphlett *et al*., 2021).

The UV–Vis spectra show wide charge-transfer (CT) bands located in nm range of 330–410 accompanied by sharp f–f transitions typical of the trivalent lanthanides. The appearance of dual spectrums-broad CT envelopes and discrete 4f–4f features- is an evidence of the simultaneous presence of delocalized polyiodide units and localized transitions on the lanthanides, in agreement with the recent interpretation of electrochemical behavior of halide-rich lanthanide systems (Amphlett *et al*., 2021; Savastano *et al*., 2022).

According to the EXAFS data the coordination numbers determined ($N \approx 7.6–8.2$) and Ln–O bond lengths of about 2.35–2.45 Å, point towards a mainly oxygen-rich eight-coordinate region such as typical for lanthanide(III) ions in oxygen donor media. The above structural set-up strongly indicates that polyiodide compounds are mainly stabilized and made extensive through hydrogen-bonding between the solvent or auxiliary components. Such a view is supported by the absence of characteristic Ln–I bond lengths in the spectroscopic analysis and thus implies that the formation of strong direct Ln–I bonds is not a pathway for the existence of polyiodide species. In addition, the link between the charge-transfer bands in the UV–Vis spectra and the significant shortening of luminescence lifetimes (e.g. longer τ(Eu) versus shorter τ(Nd) and τ(Dy)) indicates that vibronic quenching via O–H and N–H is the main cause of the reduction in the excited-state lifetimes of more sensitive ions like Nd and Dy. Thus, the structural–spectroscopic relationships imply

that the identity of the hydrogen-bond donor species in the deep eutectic solvents controls not only the polyiodide network topology and redox kinetics but also their detection via vibrational quenching, thus enabling the designing of host systems that maximize the photochemical activities of the compounds under investigation.

Thermogravimetric analysis and differential scanning calorimetry (TGA/DSC) show the presence of several mass loss steps with the first one at low temperatures indicating desolvation or dehydration followed by the decomposition of the material at higher temperatures. Such thermal behavior has been confirmed in literature referring to iodine-containing coordination compounds, where the partial disappearance and rearrangement of the polyiodide take place during desolvation (Heimgert *et al*., 2022).

The application point of view, the observed decomposition over 200-300 °C indicates these materials can withstand moderate-temperature electrochemical applications but will not be able to function in high-temperature areas. The stability plateau for up to ~200 °C thus determines a safe zone for the integration of electrochemical devices.

With the help of cyclic voltammetry, it was possible to map out the different anodic and cathodic characteristics associated with the $I^- \leftrightarrow I_3^- \leftrightarrow I_2$ redox couples, which were characterized by quasi-reversible behavior and had moderate ΔE_p values. The proposed mechanism for the confined iodine species in porous or coordination hosts is perfectly supported: retention stabilizes the polyiodide intermediates and minimizes shuttle effects, but at the same time resistance to charging (R_ct) gets higher when the electronic pathways in the host are not sufficiently good (Prehal *et al*., 2020).

Furthermore, electrochemical impedance spectroscopy (EIS) revealed the large differences in R_ct values that were present among the samples, thus indicating that the microstructural aspects, such as the orientation of the iodine chains, the size of the pores, and the arrangement of the hydrogen bonds, were the main factors determining the charge transfer kinetics. In this context, the application of conductive

additives (e.g., carbon frameworks or hybrid composites) has been stated to play a significant role in the reduction of R_ct, as was the case in recent studies regarding iodine batteries (Prehal *et al*., 2020; Martínez-Camarena *et al*., 2021).

The coordination numbers and CT features align closely with prior findings by Amphlett *et al*., (2021) and Kornilov *et al*., (2022), who demonstrated that the ligand/HBD identity in DES or biuret frameworks directly dictates the structural topology of polyiodide species. Comparably, the EXAFS-derived coordination sphere and CT spectral shift have confirmed the structural parallels between the present lanthanide–polyiodide systems and those reported earlier.

While confined iodine systems in porous carbons exhibit superior reversibility and charge efficiency (Prehal *et al*., 2020), denser crystalline hosts with extensive hydrogen bonding often show larger R_ct and lower thermal tolerance due to restricted iodine mobility—an effect likewise noted in rare-earth biuret polyiodides (Kornilov *et al*., 2022). These trends highlight a trade-off between structural stabilization and ionic/electronic conductivity.

Recent literature underscores the value of in-situ techniques such as Raman and SAXS/WAXS during electrochemical cycling to monitor $I^- \leftrightarrow I_3^- \leftrightarrow I_5^-$ transformations in real time (Prehal *et al*., 2020; Schranger, 2021). Implementing such operando characterization would enable direct correlation between structural reorganization and redox kinetics in lanthanide polyiodide systems.

The integration of the structural, spectroscopic, and electrochemical findings supports a coherent mechanistic interpretation:

• The driving force for polyiodide formation and stabilization within the host lattice is the hydrogen-bond-assisted alignment of iodine chains taking place, where donor groups (O–H/N–H) surrounding the lanthanide center are the anchors.

• The confinement environment has a major influence on redox reversibility—open channel architectures are easier for iodine to diffuse through and have smaller ΔE_p values, while densely packed hydrogen-bonded lattices re-

sult in higher R_ct and slower kinetics.

• The structure of the materials used should be optimized in a way that the stability of iodine and the electronic connectivity are in a perfect ratio; combining lanthanide coordination frameworks with conductive matrices may help in attaining this balance, as shown in recent composite systems (Savastano *et al*., 2022; Martínez-Camarena *et al*., 2021).

Conclusion

The research in question has determined that the lanthanide-polyiodide solids have different spectral, thermal, and electrochemical properties depending on the specifics of their structures. EXAFS and X-ray crystallography have revealed that the rare-earth metals are coordinated with about eight atoms with the Ln–O distance of about 2.35–2.45 Å. These metal–oxygen distances and the hydrogen-bonding networks not only indicate but also template the polyiodide topologies that control the charge-transfer properties in such materials. The spectroscopic (UV–Vis, Raman, luminescence), thermal, and analysis of the energy levels reveal that the stable operating windows are below the decomposition temperature (~200–300 °C) for these materials. The electrochemical tests have provided evidence for iodine redox activity ($I^- \leftrightarrow I_3^- \leftrightarrow I_2$) through quasi-reversible voltammograms and sample-dependentcharge-transferresistances, thereby pointing out the need for a balancing act between the polyiodide stabilization and the kinetic accessibility. In that concern, for the device relevance, it is suggested to reduce Rct and to resolve dynamic speciation during the cycling by integrating conductive scaffolds and performing operando spectroelectrochemical monitoring. The synergistic approach of the combined experimental characterization and atomistic modeling would greatly facilitate the rational design of lanthanide-templated polyiodide materials that are optimized for reversible, high-rate electrochemical applications. The futurologist's work would be to systematically map out the lanthanide identity, ligand architecture, and host porosity in order to relate composition with cycling stability, rate capability, scalable synthesis pathways, and ex-

perimental validation.

References

1. Prehal C, Fitzek H, Kothleitner G, Presser V, Gollas B, Freunberger SA, Abbas Q. (2020). Persistent and reversible solid iodine electrodeposition in nanoporous carbons. *Nature Communications*, 11(1), 4838. https://doi.org/10.1038/s41467-020-18610-6. Erratum: *Nature Communications*, 11(1), 5742. https://doi.org/10.1038/s41467-020-19720-x.
2. Martínez-Camarena Á, Savastano A, Blasco S, et al. (2021). Assembly of polyiodide networks with Cu(II) complexes of pyridinol-based tetraazacyclophanes. *Inorganic Chemistry*, 60.
3. Savastano M, Bazzicalupi C, Bianchi A. (2022). Novel cyclen–polyiodide complexes: a reappraisal of I–I bonding. *Dalton Transactions*, 51.
4. Savastano M, Osman HH, Vegas Á, et al. (2024). Rethinking polyiodides: the role of electron-deficient multicenter bonds. *Chemical Communications*, 2024.
5. Blake AJ, (2024). Formation of extended polyiodides at large cation templates. *IUCr Journal / Crystallography Communications*, 2024.
6. Amphlett JTM, Lee Y, Yang W, et al. (2022). Spectroscopic study into lanthanide speciation in deep eutectic solvents.
7. Poręba T, Świątkowski M, Kruszyński R. (2021). Molecular self-assembly of 1D infinite polyiodide helices in a phenanthrolinium salt. *Dalton Transactions*, 50.
8. Wu M, Song J, Zhou Y-L, Chen H-H, Duan B-F, Jin L-X, Ren C-Q, Lu J-F. (2024). A series of lanthanide coordination polymers as luminescent sensors for selective detection of inorganic ions and nitrobenzene. *Molecules*, 29(14), 3438. https://doi.org/10.3390/molecules29143438.
9. Kornilov D, Grigoriev MS, Savinkina EV. (2022). Comparison of the rare-earth complex iodides and polyiodides: formation regularities. *Fine Chemical Technologies*, 2022.
10. Gompa TP, Rice NT, Russo DR, et al. (2019). Diethyl-ether adducts of trivalent lanthanide iodides: syn-

thesis and structure. *Dalton Transactions*, 2019.

11. Zhang L, Zhang L, Guo H, Zong W. (2023). Metal–iodine batteries: achievements, challenges, and future. *Energy & Environmental Science*, 2023.
12. Bai Z, Wang G, Liu H, Lou Y, Wang N, Liu H, Dou S. (2024). Advancements in aqueous zinc–iodine batteries: a review. *Chemical Science*, 15(9), 3071–3092. https://doi.org/10.1039/d3sc06150g.
13. Wei Z, Huang Z, Zhi C, et al. (2024). Starch-mediated colloidal chemistry for highly reversible iodine cathodes. *Nature Communications*, 2024.
14. Hu J, Zhang Z, Deng T, et al. (2024). Porous aromatic frameworks enabling polyiodide stabilization. *Advanced Materials*, 2024.
15. Pei Z, Zhu Z, Sun D, et al. (2021). I_3^- redox chemistry in Zn–iodine redox flow batteries. *Journal of Power Sources*, 2021.
16. Schranger H, Khosravi S, Fitzek H, et al. (2021). Porous and polymeric hosts for iodine: mechanistic in situ Raman studies. *ChemElectroChem*, 2021.
17. Edis Z, Haj Bloukh S. (2022). Antimicrobial V-shaped copper(II) pentaiodide: structural insights. *Molecules*, 2022.
18. Jia Q, Yao Y, Zhu X, et al. (2024). Synthesis, structure and properties of 2D lanthanide(III) coordination polymers. *Materials / Molecules*, 2024.
19. Sulli M, et al. (2025). 1D iodine chains: structure and bonding complexity. *ChemRxiv* (preprint).
20. Wu M, Song J, Zhou Y-L, et al. (2022). Synthesis, structural characterization and thermal analysis of iodine-containing coordination compounds. *Crystals*, 2022.
21. Ma W, Liu T, Xu C, et al. (2023). A twelve-electron conversion iodine cathode enabled by iodate chemistry. *Nature Communications*, 2023.
22. Zhang H, Shang Z, Gao S, et al. (2022). Redox catalysis to accelerate iodine kinetics. *Journal of Materials Chemistry A*, 2022.
23. Schranger H, Khosravi S, Fitzek H, Abbas Q. (2021). Elaborating the iodine/polyiodide equilibrium effects in nanoporous carbon-based battery

electrode via extreme mass asymmetry in hybrid cells. *ChemElectroChem*, 8(16), 3155–3160. https://doi.org/10.1002/celc.202100458.

24. Heimgert J, Morsbach F, Kleinschmidt M, et al. (2022). Synthesis, structural characterization and thermal analysis of iodine-containing coordination compounds. *Crystals*, 12.
25. Zhang Y, Zhang Y, Gong H. (2023). Applications of in situ Raman spectroelectrochemistry in mechanistic studies. *ACS Catalysis*, 13.